Communication

Dual-Mode Compression of Dipole Antenna by Loading Electrically Small Loop Resonator

Weiquan Zhang, Yue Li, Ziheng Zhou, and Zhijun Zhang

***Abstract*— This communication presents a dual-mode dipole antenna for impedance bandwidth improvement. In our approach, an electrically small loop (ESL) resonator is properly loaded to compress the operating frequencies of first- and third-order modes. With the existence of ESL, the third-order mode shifts to its first-order mode to obtain a wide bandwidth with stable polarization and radiation patterns, due to the fact that ESL is equivalent to an orthogonal magnetic dipole at the third-order mode. To validate the design strategy, a prototype was fabricated and tested. Omnidirectional radiation pattern in H-plane is achieved over the entire operating band from 2.94 to 3.89 GHz while keeping a smaller size of $0.45\lambda_0 \times 0.17\lambda_0$ (λ_0 is the wavelength in free space at the center frequency). Good agreement has been obtained between measurement and simulation.**

***Index Terms*— Antenna input impedance, broadband antennas, dipole antennas, electrically small loop (ESL).**

I. Introduction

Wideband dipole antennas with compact dimensions and stable radiation patterns over their operating frequency bands are widely used in modern communication services such as the fifth-generation mobile networks, WiMax, Wi-Fi, and so on. One approach to enhance the bandwidth of dipole antennas is to adopt multiple dipoles with different lengths for different resonant frequencies [1]–[5]. These antennas are usually bulky and complex in geometry for fabrication and each dipole works with its single mode. A multimode method is proposed to enhance the bandwidth [6], [7]. Parasitic linear dipole [6] and parasitic loop [7] are added to broaden the bandwidth by creating new resonant modes. In [8], an artificial mu-negative transmission line (MNG-TL) structure is realized for wide bandwidth but with larger size. On the other hand, slot antenna is another candidate for wideband wireless communications because of its simple and planar structure. Stub slots are added along the main slots in [9], [10] to shift the third-order mode down to the first-order mode for dual-mode operation but with unstable radiation patterns across their operating bandwidth. As an effective approach, theory of characteristic modes (TCMs) [11]–[13] is used to design wideband dipole antennas [7], [14]. The TCM provides an analytical insight of the radiating modes on the dipole structure. By introducing loaded stubs along the dipole near the current nulls of the fifth-order mode, the fifth-order mode shifts to its third-order mode for achieving a wideband operation [14].

Manuscript received July 12, 2019; revised September 17, 2019; accepted September 20, 2019. Date of publication October 28, 2019; date of current version April 7, 2020. This work was supported in part by the National Natural Science Foundation of China under Grant 61771280, in part by the Natural Science Foundation of Beijing Manipulate under Contract 4182029, and in part by the Tsinghua University Initiative Scientific Research Program under Contract 2019Z08QCX16. *(Corresponding author: Yue Li.)*

The authors are with the Department of Electronic Engineering, Tsinghua University, Beijing 100084, China, and also with the Beijing National Research Center for Information Science and Technology, Tsinghua University, Beijing 100084, China (e-mail: lyee@tsinghua.edu.cn).

Color versions of one or more of the figures in this communication are available online at http://ieeexplore.ieee.org.

Digital Object Identifier 10.1109/TAP.2019.2948712

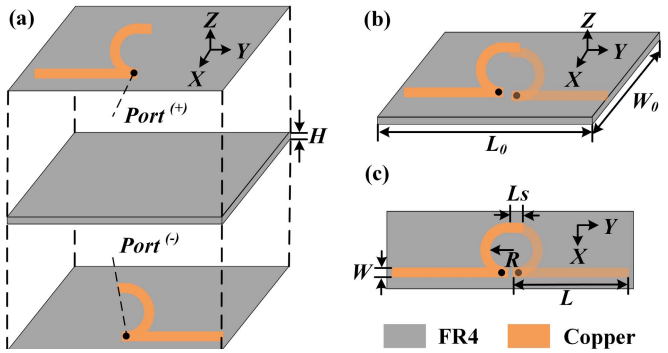

Fig. 1. General structure of the proposed antenna. (a) Layered, (b) perspective, and (c) top views with geometry parameters.

As another key property, stable radiation pattern is achieved by using the magnetoelectric dipole antenna in [15]. By combing a pair of electric and magnetic dipoles, stable radiation patterns are realized over the entire operating band. Multidipole antenna is also an efficient way to achieve stable radiation patterns. Through a rational design of position of dipoles and reflector, an antenna with stable radiation patterns is obtained [4]. Other dipole antenna designs with stable radiation patterns have been investigated and designed [16], [17]. A wideband segmented dipole antenna with stable radiation patterns is realized by adding interlaced coupling lines at each section [16]. Stable radiation patterns are achieved in [17] with a simple cylindrical cavity.

In this communication, a dual-mode dipole antenna with electrically small loop (ESL) load is proposed for the merits of wide bandwidth, stable radiation patterns, and smaller size. By loading an ESL, the current length of the third-order mode is lengthened and as a result, the first- and third-order modes are compressed for wideband requirement. Meanwhile, the proposed antenna is with stable polarization and radiation patterns in wide bandwidth, since ESL is equivalent to an orthogonal magnetic dipole at the resonant frequency of the third-order mode. The impedance matching and key parameters are also investigated to obtain an optimized performance. A prototype is fabricated to provide an experimental verification of the idea. The proposed antenna can achieve an impedance bandwidth of 27.8% (SWR $<$ 2) from 2.94 to 3.89 GHz while keeping a smaller size of $0.45\lambda_0 \times 0.17\lambda_0$. Meanwhile, as the first- and third-order modes are with similar omnidirectional radiation patterns, stable radiation patterns in H-plane are achieved within the overall operation bandwidth.

II. Antenna Design and Analysis

Fig. 1 presents the geometry of the proposed dual-mode dipole antenna on an FR4 substrate with relative permittivity $\varepsilon_r = 4.4$ and loss tangent of 0.02. The proposed antenna consists of a straight

TABLE I
DETAILED DIMENSION OF THE PROPOSED ANTENNA

Parameter	Value(mm)	Parameter	Value(mm)
L	18.5	Ls	0.47
W	1	W_0	15
R	3.5	L_0	40
H	1		

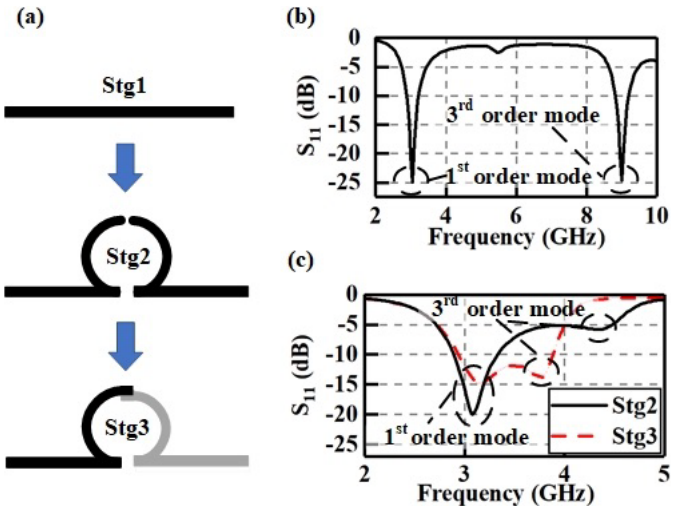

Fig. 2. (a) Development stages of the proposed electrically small loop (ESL)-loaded dipole antenna and $|S_{11}|$ corresponded to (b) stage 1 and (c) stages 2 and 3.

dipole and an ESL ($k_0 R \approx 0.25$, k_0 is the wavenumber in free space at the center frequency) as shown in Fig. 1(b). The proposed antenna is divided into two sections and exhibits even-symmetrical property along the xz plane. They are printed in the top and bottom layers separately, as shown in Fig. 1(a). Fig. 1(c) depicts the top view of the dipole antenna. The overlap length of the ESL is Ls, which is the key parameter for impedance bandwidth improvement. Table I lists the detailed dimensions. Due to the center-fed scheme, all the even-order radiation modes are unable to be excited in theory. In this communication, the first- and third-order modes are compressed so that they are close to each other for wideband operation. The resonant frequency of the second-order mode is decreased simultaneously as the third-order mode is compressed. The resonant frequency of the second-order mode is corresponding to the worst impedance matching point between the resonant frequencies of the first- and third-order modes.

The design guideline is given as follows.

1) Based on the target frequency (f_0), select the length (L) of straight dipole as $0.5\lambda_0$ initially since the straight dipole is responsible for the first-order mode.
2) Since the third-order mode is compressed to target frequency f_0, the electrical size of the antenna at the third-order mode is based on λ_0 here. According to the current distribution of the third-order mode, the circumference ($2\pi R$) of ESL is selected as $0.25\lambda_0$, so as to keep the current distribution of the straight dipole in the same direction.
3) The value of L is fine-tuned to obtain a proper resonant frequency of the first-order mode and then the values of R and L are fine-tuned to obtain the widest achievable impedance bandwidth.

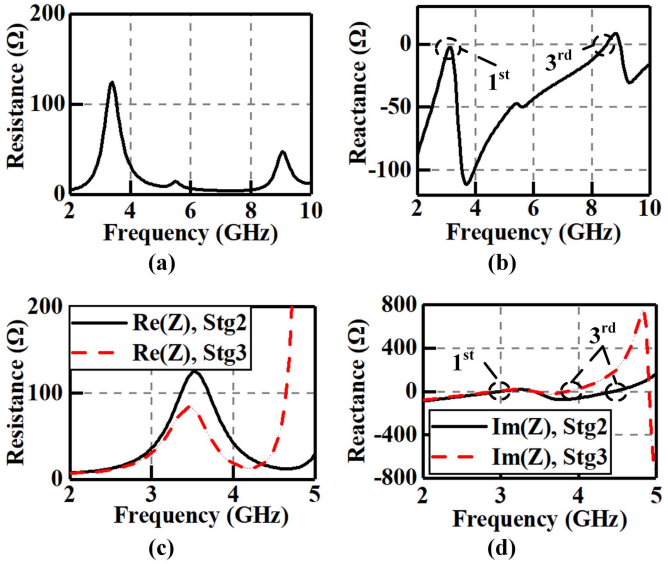

Fig. 3. (a) Resistance and (b) reactance characteristics at stage 1, (c) resistance and (d) reactance characteristics at stages 2 and 3.

The antenna development stages are shown in Fig. 2(a). In the second design stage, an ESL is loaded with break points, so as to lengthen the current of the third-order mode for compressing. In the final design stage, the two half symmetrical sections of dipole antenna are printed separately at the top and bottom layers. Meanwhile, the overlap of ESL is used to improve impedance matching through field coupling. Fig. 2(b) and (c) displays the $|S_{11}|$ for development stages. The results are simulated by HFSS [18]. From Fig. 2(b), it is found that the first two odd modes of a straight dipole locate at 3.05 and 9 GHz, respectively. With the existence of ESL, the resonant frequency of the third-order mode moves down to 4.35 GHz as shown in Fig. 2(c). The reason of this phenomenon is that the current third-order mode is lengthened by the loading ESL. In stage 3, the resonant frequency of the third-order mode shifts to its first mode and the bandwidth (SWR $<$ 2) is enhanced from 11.18% to 27.8%. Therefore, ESL overlap decreases the resonant frequency of the third-order mode further and improves impedance matching. It has been noted that the proposed dipole antenna resonates at 3.16 and 3.76 GHz finally. It is shown that the third-order mode shifts to 3.76 GHz, while the first-order mode is changed slightly. Therefore, first- and third-order modes are compressed effectively by loading an ESL.

To further reveal its operation principle, the proposed antenna is investigated by its input impedance. The frequency responses of the input impedance in different stages are depicted in Fig. 3. As shown in Fig. 3(a) and (c), the input resistance within the considered bandwidth in stages 1 and 2 is higher than that in stage 3. This phenomenon indicates that the overlap of ESL improves the impedance matching. As illustrated in Fig. 3(b), the reactance null point ($\mathrm{Im}(Z) = 0$) of the third-order mode is around 9 GHz. Then the third-order mode moves down to 4.35 GHz with ESL load and further shifts to the first-order mode with the overlap of ESL as Fig. 3(d) depicts. Thus, a wideband characteristic with two reactance null points can be obtained by loading an ESL.

The current distributions of the two resonant modes of the proposed dipole antenna with ESL load are shown in Fig. 4. According to Fig. 4(a), the straight dipole resonates at first-order mode and its current amplitude is larger than that in ESL. Hence, the straight dipole

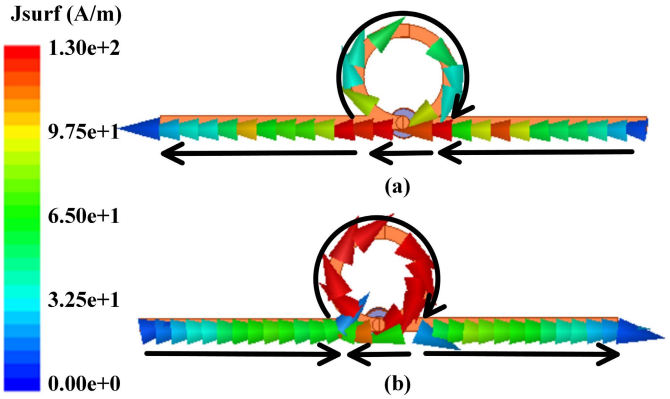

Fig. 4. Current distributions at (a) 3.16 and (b) 3.76 GHz.

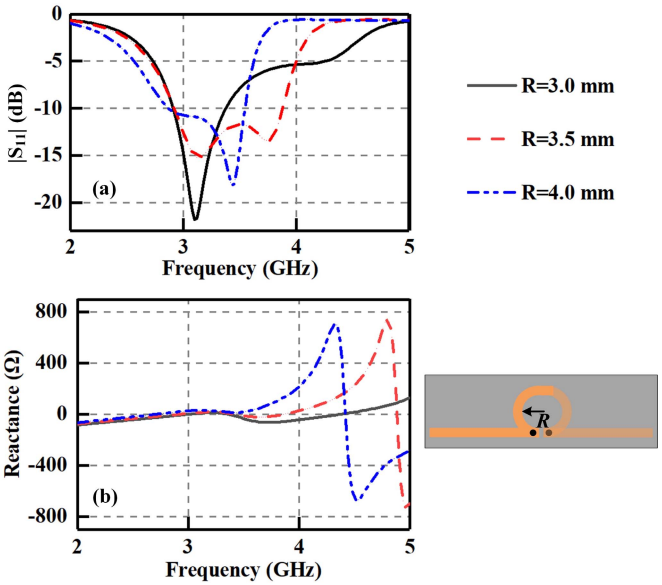

Fig. 5. (a) Variation in resonant frequencies and (b) reactance characteristics of the proposed antenna with respect to radius R.

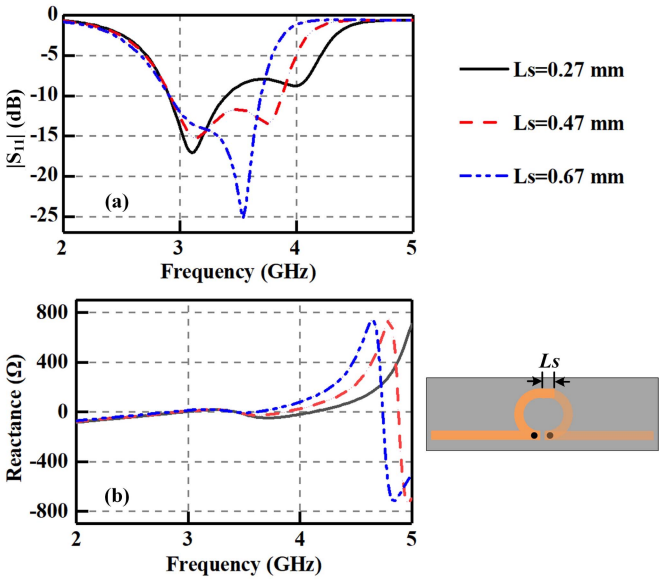

Fig. 6. (a) Variation in resonant frequencies and (b) reactance characteristics of the proposed antenna with respect to length Ls.

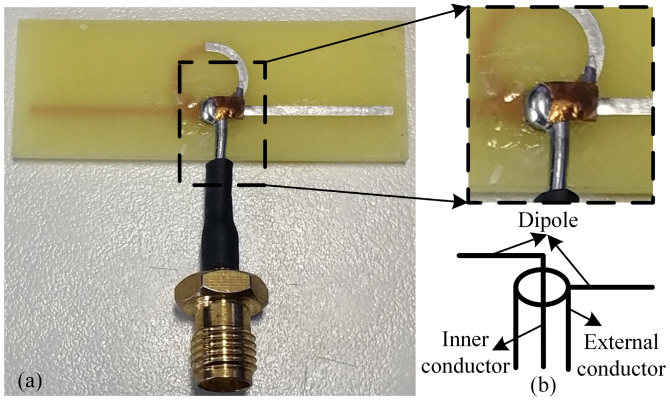

Fig. 7. (a) Fabricated prototype of the proposed antenna and (b) schematic of the feeding structure.

is responsible for the radiation at 3.16 GHz. As we know, the middle current direction of third-order mode on a dipole is opposite to that on both sides. Hence, the middle section of a dipole antenna performs as an ESL here to lengthen the current at 3.76 GHz as depicted in Fig. 4(b). As a result, the resonant frequency of third-order mode is decreased and the mode compression of a dipole antenna is achieved for broadband operation. As shown in Fig. 4(b), the current amplitude on ESL is almost uniform at the third-order mode, and ESL is equivalent to an orthogonal magnetic dipole at the third-order mode in theory and as a result, stable polarization and radiation patterns are obtained. Besides, ESL has null compensation effect on radiation patterns in E-plane.

To provide a design guidance of the proposed antenna with ESL load, a parametric study was conducted to investigate the effects of various parameters. The effect of parameter R on $|S_{11}|$ is shown in Fig. 5, by varying it from 3.0 to 4.0 mm with 0.5 mm step in the range. It can be observed from Fig. 5(a) that as R increases, the third-order mode definitely decreases, whereas the first-order mode changes slightly. This phenomenon is corresponding to the reactance null point of the third-order mode that moves down to lower frequency as shown in Fig. 5(b). Resistance characteristics (not shown here for brevity) change slightly with respect to radius R. Therefore, ESL has strong effect on the third-order mode than on the first-order mode because ESL works as the middle section of the third-order mode. However, when R is big enough that the circumference of ESL is comparable to the length of the straight dipole, the analysis above is inapplicable. To obtain a better impedance matching, $R = 3.5$ mm is selected.

Besides, the effect of the overlap length is studied here. Fig. 6(a) and (b) depict the reflection coefficient and the input reactance with respect to different overlap lengths. The results show that the resonant frequency of the third-order mode and reactance characteristics are affected by the length Ls, while those of the first-order mode almost are unaffected. As Ls increases, the operating frequency of the third-order mode moves down as shown in Fig. 6. Therefore, the third-order mode can be tuned individually by changing the length of the overlap only.

III. Measurement Results and Validation

In this section, the proposed ESL-loaded dipole antenna is fabricated and measured to verify the approach. The prototype is shown in Fig. 7, which is fed by 50 Ω coaxial cable. Reflection coefficient of the antenna is measured using an N5071B vector network analyzer (300 kHz–9 GHz), the gains and radiation patterns are measured

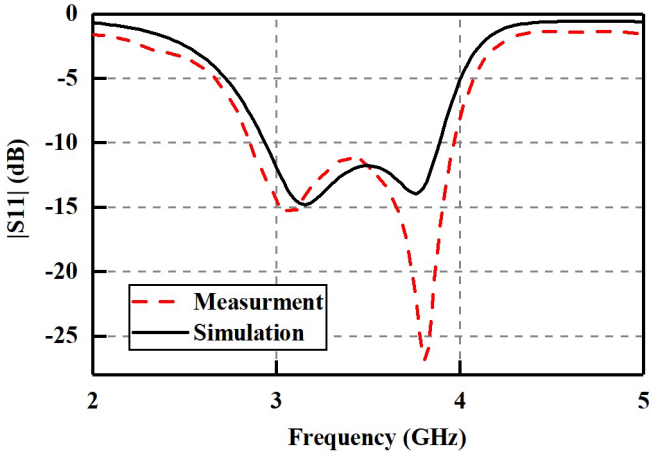

Fig. 8. Simulated and measured reflection coefficient values $|S_{11}|$ of the proposed dipole antenna with electrically small loop (ESL) loading.

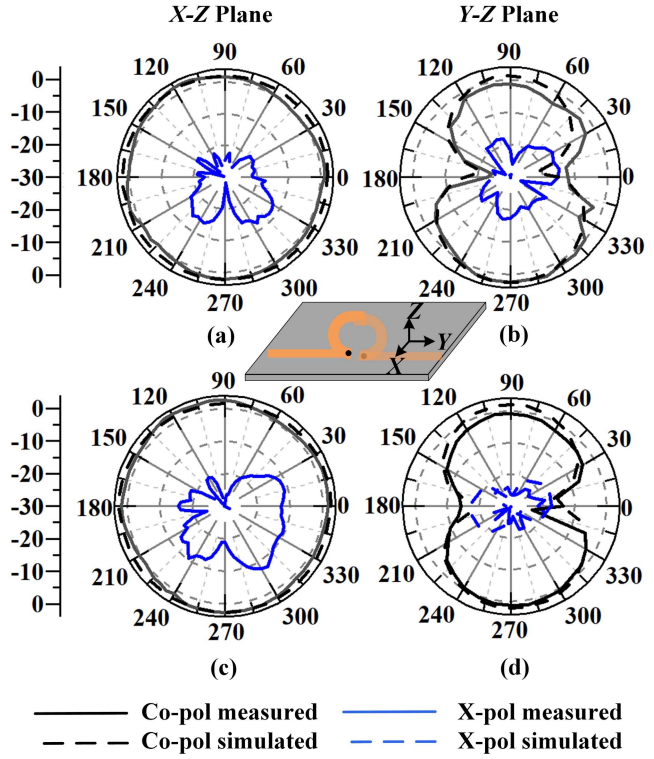

Fig. 9. Measured and simulated radiation patterns of the proposed antenna at different frequencies. (a) 3.2 GHz, *xz* plane. (b) 3.2 GHz, *yz* plane. (c) 3.6 GHz, *xz* plane. (d) 3.6 GHz, *yz* plane.

in a far field anechoic chamber. Fig. 8 shows the measured and simulated reflection coefficients. It is shown that the measured data in general agree well with the simulated results. Only a little shifting of the matching frequencies occurs for the measured data compared to the simulated results. The disagreement between the measurement and simulation is caused by the unbalanced SMA connector, such as the unwanted surface unevenness, and fabrication error, such as the imprecise welding between the coaxial cable and antenna. The impedance bandwidth ($S_{11} \leq -10$ dB) of the proposed antenna were simulated and measured as 0.95 (2.94–3.89 GHz) and 1.11 GHz (2.86–3.97 GHz), respectively.

The measured and simulated radiation patterns of the fabricated prototypes at 3.2 and 3.6 GHz are shown in Fig. 9, with good agreement between simulation and measurements. Measurements

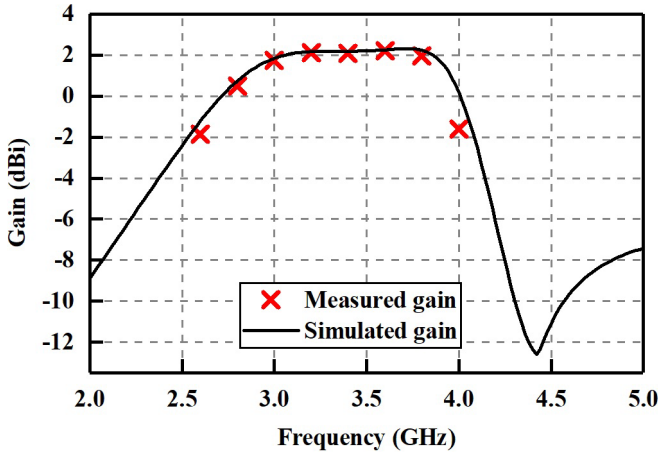

Fig. 10. Simulated and measured gains of the proposed antenna.

TABLE II
COMPARISON AMONG THE PROPOSED ANTENNAS WITH DUAL-MODE DIPOLE

Reference	Modes	Method	BW(%)	Size (λ_0^2)
[7]	Two resonators	Parasitic loop	44.2	0.63×0.32
[10]	Slot 1^{st}+3^{rd}	Stub-loaded	31.5	1.32×1.32
[14]	Dipole 3^{rd}+5^{th}	Stub-loaded	11.2	1.04×0.83
Our Work	Dipole 1^{st}+3^{rd}	Loop-loaded	27.8	0.45×0.17

at other operating frequencies across the bandwidth also show radiation patterns similar to those plotted here. From these results, it is clear that a good omnidirectional radiation pattern in H-plane (*xz* plane), with small gain variations of less than 2.9 and 1.75 dB at 3.2 and 3.6 GHz, respectively, are obtained. Therefore, a wideband ESL-loaded dipole antenna with stable omnidirectional radiation patterns is achieved. It can be seen that the two null points of eight-shaped radiation patterns in *yz* plane are not as small as those of the ordinary dipoles. The reason for this phenomenon is that the null compensation is caused by ESL, especially around the resonant frequency of the third-order mode.

The radiation characteristics of the fabricated prototype were also studied. The radiation gains are presented in Fig. 10 as a function of frequency. It is seen that the measured results agree well with the simulated ones. It can be observed that the antenna exhibits stable gain frequency response within their impedance bandwidth. The average gain of the proposed dipole is greater than 2 dBi. The efficiency of the ESL-loaded antenna is better than 79% within the overall bandwidth. The maximum and minimum efficiencies are 94.67% at 3.22 GHz and 79.7% at 3.89 GHz, respectively.

Table II shows a comparison between the existing designs and our work. With reference to Table II, the proposed antenna has smaller size than the previous designs [7], [10], [14], as the two lowest odd modes are combined; and in our work, ESL load was chosen rather than stub load. A parasitic loop is used to create a new resonant mode so as to widen the bandwidth in [7], while the ESL in this communication is used to compress the third-order mode mainly. The slot antenna in [10] exhibits wider bandwidth but with largest size and unstable radiation patterns across their operating

frequency bandwidth. And the stub-loaded dipole proposed in [14] has the narrowest bandwidth. In summary, our design exhibits better performance in terms of smaller size compared to the reference dipole antennas with available bandwidth.

IV. Conclusion

The design of a dual-mode antenna with ESL load for impedance bandwidth improvement has been introduced in this communication. By loading an ESL, the current length of the third-order mode is lengthened to compress the third-order mode for dual-mode operation. Besides, the ESL is equivalent to an orthogonal magnetic dipole at the third-order mode and as a result, stable polarization and radiation patterns are obtained. It is seen that the proposed ESL-loaded dipole antenna could achieve a fractional bandwidth of up to 27.8% against 11.18% in a single-mode dipole. A parametric study has been carried out to devise a design guideline for the ESL-loaded dipole antenna. An ESL-loaded antenna was also fabricated and measured. The measured results were found to agree well with the simulated data. The fabricated prototype can provide a wide effective bandwidth of about 1.11 GHz (2.86–3.97 GHz) with VSWR 2:1 impedance matching and the stable omnidirectional radiation patterns in H-plane while keeping smaller size of $0.45\lambda_0 \times 0.17\lambda_0$. Therefore, the proposed approach should be useful to explore other types of multimode antennas, and the proposed antenna in a simple form is ideally a practical element for a wideband array antenna with stable omnidirectional radiation patterns.

References

[1] C. A. Balanis, *Antenna Theory: Analysis and Design*, 3rd ed. Hoboken, NJ, USA: Wiley, 2005.

[2] R. Duhamel and F. Ore, "Logarithmically periodic antenna designs," in *Proc. IRE Int. Conv. Rec.*, vol. 6, Mar. 1966, pp. 139–151.

[3] D. Isbell, "Log periodic dipole arrays," *IRE Trans. Antennas Propag.*, vol. 8, no. 3, pp. 260–267, May 1960.

[4] Q.-X. Chu and Y. Luo, "A broadband unidirectional multi-dipole antenna with very stable beamwidth," *IEEE Trans. Antennas Propag.*, vol. 61, no. 5, pp. 2847–2852, May 2013.

[5] Y. Luo and Q.-X. Chu, "Oriental crown-shaped differentially fed dual-polarized multidipole antenna," *IEEE Trans. Antennas Propag.*, vol. 63, no. 11, pp. 4678–4685, Nov. 2015.

[6] O. Aboderin, L. M. Pessoa, and H. M. Salgado, "Wideband dipole antennas with parasitic elements for underwater communications," in *Proc. OCEANS-Aberdeen*, Jun. 2017, pp. 1–6.

[7] D.-L. Wen, Y. Hao, H.-Y. Wang, and H. Zhou, "Design of a wideband antenna with stable omnidirectional radiation pattern using the theory of characteristic modes," *IEEE Trans. Antennas Propag.*, vol. 65, no. 5, pp. 2671–2676, May 2017.

[8] K. Wei, Z. Zhang, Z. Feng, and M. F. Iskander, "A wideband MNG-TL dipole antenna with stable radiation patterns," *IEEE Trans. Antennas Propag.*, vol. 61, no. 5, pp. 2418–2424, May 2013.

[9] W.-J. Lu and L. Zhu, "A novel wideband slotline antenna with dual resonances: Principle and design approach," *IEEE Antennas Wireless Propag. Lett.*, vol. 14, pp. 795–798, 2015.

[10] W.-J. Lu and L. Zhu, "Wideband stub-loaded slotline antennas under multi-mode resonance operation," *IEEE Trans. Antennas Propag.*, vol. 63, no. 2, pp. 818–823, Feb. 2015.

[11] R. J. Garbacz and R. Turpin, "A generalized expansion for radiated and scattered fields," *IEEE Trans. Antennas Propag.*, vol. AP-19, no. 3, pp. 348–358, May 1971.

[12] R. F. Harrington and J. R. Mautz, "Theory of characteristic modes for conducting bodies," *IEEE Trans. Antennas Propag.*, vol. AP-19, no. 5, pp. 622–628, Sep. 1971.

[13] R. F. Harrington and J. R. Mautz, "Computation of characteristic modes for conducting bodies," *IEEE Trans. Antennas Propag.*, vol. AP-19, no. 5, pp. 629–639, Sep. 1971.

[14] Y. Luo, Z. N. Chen, and K. Ma, "Enhanced bandwidth and directivity of a dual-mode compressed high-order mode stub-loaded dipole using characteristic mode analysis," *IEEE Trans. Antennas Propag.*, vol. 67, no. 3, pp. 1922–1925, Mar. 2019.

[15] K. M. Luk and H. Wong, "A new wideband unidirectional antenna element," *Int. J. Microw. Opt. Technol.*, vol. 1, no. 1, pp. 2098–2101, Jul. 2006.

[16] X. Jia and D. Piao, "A wideband segmented line dipole antenna with stable radiation patterns," in *Proc. 11th Int. Symp. Antennas, Propag. EM Theory (ISAPE)*, Guilin, China, Oct. 2016, pp. 22–24.

[17] Z. Tu, D.-F. Zhou, G.-Q. Zhang, F. Xing, X. Lei, and D.-W. Zhang, "A wideband cavity-backed elliptical printed dipole antenna with enhanced radiation patterns," *IEEE Antennas Wireless Propag. Lett.*, vol. 12, pp. 1610–1613, 2013.

[18] Ansoft Corp., Pittsburgh, PA, USA. *HFSS V15*. Accessed: Nov. 1, 2019. [Online]. Available: http://www.ansys.com/products/electronics/ansys-hfss